ACSNANO

www.acsnano.org

ARTICLE

Chemo-Mechanically Operating Palladium-Polymer Nanograting Film for a Self-Powered H_2 Gas Sensor

Min-Ho Seo,[▽] Kyungnam Kang,[▽] Jae-Young Yoo,[▽] Jaeho Park, Jae-Shin Lee, Incheol Cho, Beom-Jun Kim, Yongrok Jeong, Jung-Yong Lee, Byeongsu Kim, Junsuk Rho,* Jun-Bo Yoon,* and Inkyu Park*

Cite This: *ACS Nano* 2020, 14, 16813–16822

Read Online

ACCESS | Metrics & More | Article Recommendations | Supporting Information

ABSTRACT: This study proposes a reliable and self-powered hydrogen (H_2) gas sensor composed of a chemo-mechanically operating nanostructured film and photovoltaic cell. Specifically, the nanostructured film has a configuration in which an asymmetrically coated palladium (Pd) film is coated on a periodic polyurethane acrylate (PUA) nanograting. The asymmetric Pd nanostructures, optimized by a finite element method simulation, swell upon reacting with H_2 and thereby bend the PUA nanograting, changing the amount of transmitted light and the current output of the photovoltaic cell. Since the degree of warping is determined by the concentration of H_2 gas, a wide concentration range of H_2 (0.1−4.0%) can be detected by measuring the self-generated electrical current of the photovoltaic cell without external power. The normalized output current changes are ∼1.5%, ∼2.8%, ∼3.5%, ∼5.0%, ∼21.5%, and 25.3% when the concentrations of H_2 gas are 0.1%, 0.5%, 1.0%, 1.6%, 2%, and 4%, respectively. Moreover, because Pd is highly chemically reactive to H_2 and also because there is no electrical current applied through Pd, the proposed sensor can avoid device failure due to the breakage of the Pd sensing material, resulting in high reliability, and can show high selectivity against various gases such as carbon monoxide, hydrogen sulfide, nitrogen dioxide, and water vapor. Finally, using only ambient visible light, the sensor was modularized to produce an alarm in the presence of H_2 gas, verifying a potential always-on H_2 gas monitoring application.

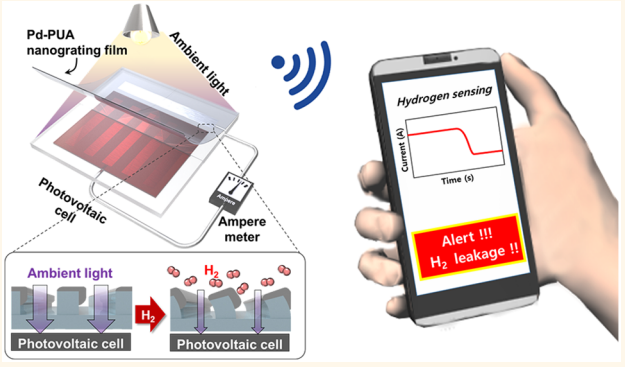

KEYWORDS: *hydrogen sensor, palladium, nanograting, nanotransducer, self-powered sensor*

Recently, hydrogen (H_2) has attracted great attention in the energy and environmental fields because it can be used as an efficient energy storage method with high-energy density, cleanliness, and ease of distribution.[1,2] H_2 gas is also used in various industrial applications, including petroleum and glass refining, semiconductor and pharmaceutical manufacturing, H_2-cooled systems, and metallurgic processes.[3−6] Although H_2 gas can be used in many industrial applications and fuel cells, its leakage needs to be continuously monitored because the colorless and odorless H_2 gas has a low explosive limit of 4% at room temperature.[7−10] Therefore, H_2 gas sensors with high response, high selectivity, low cost, low power consumption, and high reliability are essential to ensure the safety of H_2 gas, with power consumption and reliability being the most important concerns for continuous sensor operation.

Existing gas sensors include catalytic combustion sensors,[11] optical sensors,[12] chemo-resistive sensors,[4,13−19] *etc.* Catalytic combustion types require a heat source for gas detection because they operate in response to the combustion of a target gas with the help of catalysts, and thus they consume relatively large electrical power.[20,21] For these reasons, optical-type H_2 gas sensors have the advantage of low electrical power consumption because they respond to changes in the optical properties induced by the gas reactions; however, they absolutely require a

Received: July 2, 2020
Accepted: November 24, 2020
Published: December 2, 2020

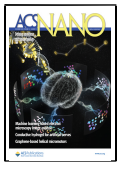

https://dx.doi.org/10.1021/acsnano.0c05476
ACS Nano 2020, 14, 16813−16822

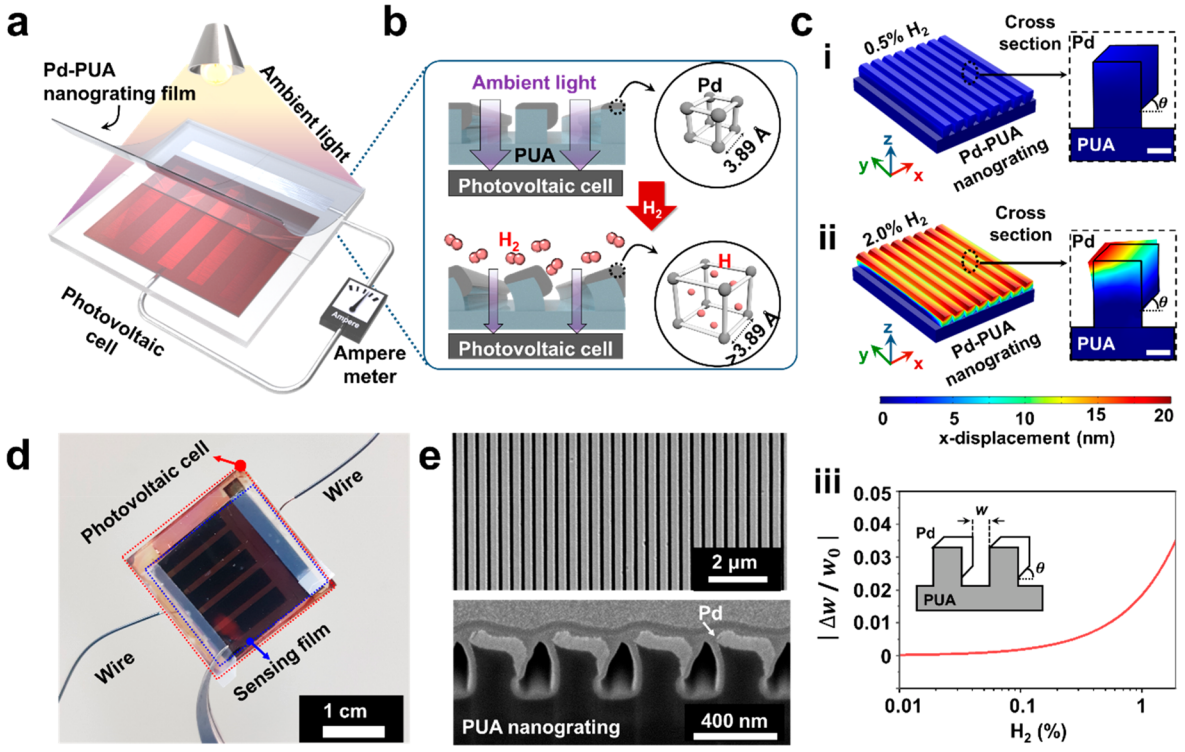

Figure 1. (a) Schematic illustration of the self-powered H_2 gas sensor structure and (b) H_2 gas detection principle according to volume expansion of Pd on the PUA nanograting. (c) FEM simulation results for Pd-PUA nanograting film by volumetric expansion of Pd in (i) 0.5% and (ii) 2% H_2 gas environments. (iii) The rate of change in the Pd gap of the Pd-PUA nanograting film ($|\Delta w/w_0|$) according to the concentration of H_2 gas. (d) Optical image of fabricated self-powered H_2 gassensor. (e) SEM images of Pd-PUA nanograting film. Top and cross-sectional images are in upper and lower panels, respectively.

separate light source and photodetector, making the total system size large. This size issue prevents the use of optical H_2 sensors in various mobile applications. In contrast, chemo-resistive-type sensors (metal oxide, carbon nanotube, conductive polymer, metal, *etc.*) have been widely used because of their compact size, simple operation principle, low cost, and high response.[4,22−27] Moreover, recent advances in chemo-resistive sensors that exploit micro-electromechanical systems (MEMS) platforms have significantly reduced the electrical power consumption.[20,28] Nevertheless, their manufacturing process is very complicated, and the power consumption is still at several mW.

As reliable and power-efficient H_2 sensors with high scalability, palladium (Pd)-based chemo-resistive sensors have attracted much attention because they are able to selectively detect H_2 gas at room temperature.[25,29] When H_2 gas molecules come in contact with Pd, H_2 is divided into hydrogen atoms on the surface of the Pd metal and enters into the Pd lattice to form PdH_x.[13,18,30,31] This phenomenon causes both a change in the electrical resistance and volume expansion of the Pd.[29] Although Pd-based chemo-resistive gas sensors have significantly reduced electrical power consumption, electrical power is still necessary for the sensor operation. Thus, the use of Pd sensors in diverse applications that require the continuous monitoring of H_2 gas is still limited (Supporting Information, Table S1). More importantly, repeated reactions of Pd with H_2 can generate mechanical fractures and electrical shortages due to volumetric expansion and electro-migration at grain boundaries, which result in poor sensor reliability.[32,33] Therefore, an ultralow-power and reliable H_2 sensor must be developed to ensure constant monitoring and safe use of H_2 gas.

This article presents a reliable and self-powered H_2 sensor that employs a chemo-mechanically operated Pd-polymer nanograting film combined with a photovoltaic cell. This sensor can detect H_2 gas by detecting changes of the optical transparency through the nanograting film caused by mechanical deformation of the Pd-polyurethane acrylate (PUA) nanograting when it is exposed to the H_2 gas. Most importantly, the proposed gas sensor can be self-powered without an additional external power source for H_2 gas detection, unlike conventional sensors such as catalytic combustion sensors, optical sensors, and chemo-resistive sensors. This is because not only the proposed sensor generates a current output depending on the H_2 gas concentration but also the electric current generated by the photovoltaic cell can be used as the power source. To optimize the sensor performance, the most favorable deposition angle and thickness of Pd were studied by finite element method (FEM) simulation and experiments. The fabricated sensor was capable of sensing H_2 gas in a wide concentration range (from 0.1 to 4%) and exhibited highly stable and repeatable gas sensing performance over 125 cycles up to a concentration of 2% H_2. Moreover, the sensor shows a high selectivity to H_2 gas against carbon monoxide (CO), hydrogen sulfide (H_2S), and nitrogen dioxide (NO_2) gases as well as against water vapor (H_2O). Finally, using only ambient visible light, the sensor was modularized to produce an alarm in the presence of H_2 gas.

RESULTS AND DISCUSSION

Figure 1a presents a schematic illustration of the proposed self-powered H_2 sensor device. The proposed sensor device is configured as a laminated Pd-PUA nanograting film on a photovoltaic cell (left panel in Figure 1a). In particular, the Pd-

https://dx.doi.org/10.1021/acsnano.0c05476
ACS Nano 2020, 14, 16813−16822

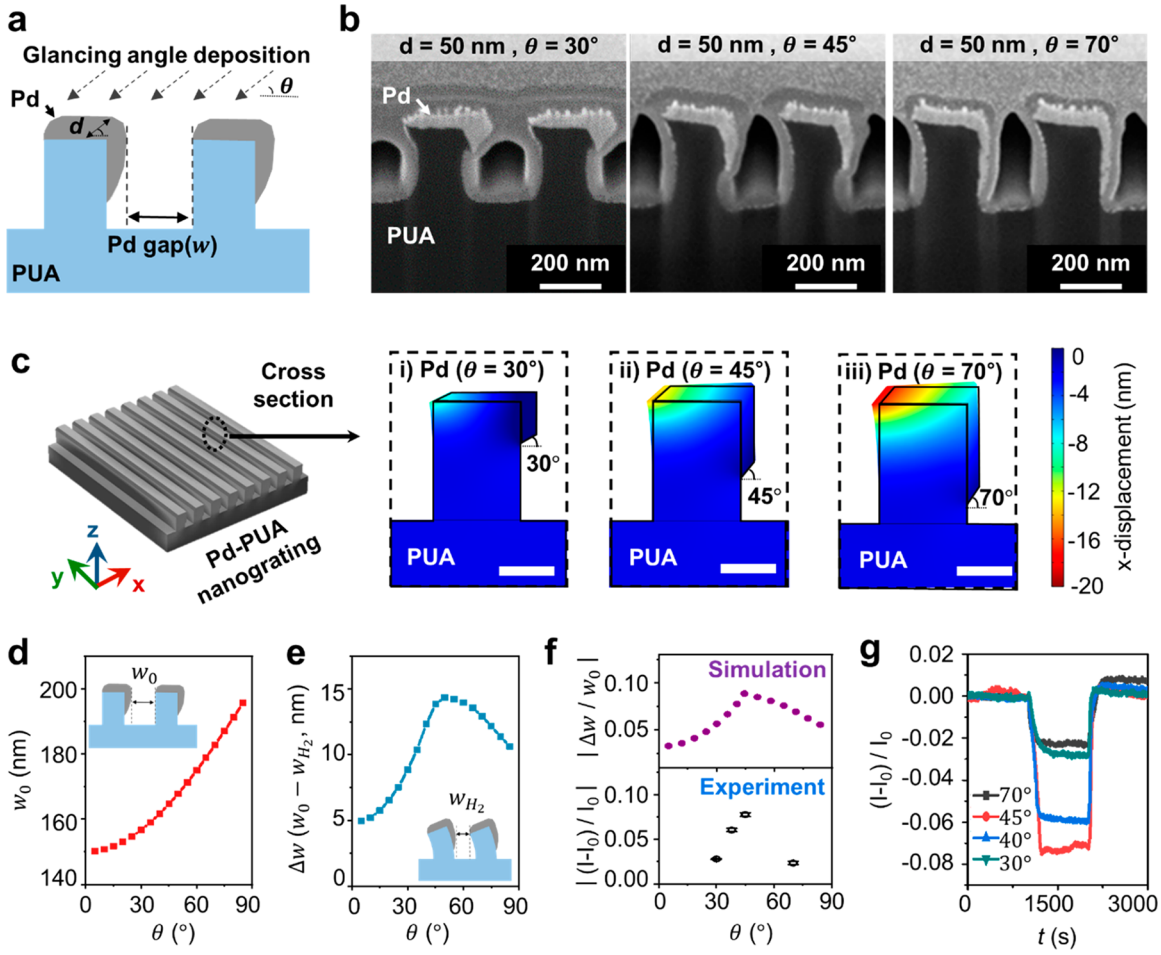

Figure 2. (a) Schematic of Pd-PUA nanograting. (b) FIB-SEM image of fabricated Pd-PUA nanograting according to various deposition angles (θ). (c) FEM simulation results for the deformation of Pd-PUA nanograting film in the 2% H_2 gas. The *x*-axial displacement is presented with a rainbow color-map (scale bar = 100 nm). (d) Pd gap of Pd-PUA nanograting according to deposition angle. (e) Simulation results of PUA deformation produced by Pd expansion at various deposition angles. (f) Simulation and experimental results for 2% H_2 gas detection of self-powered gas sensors with various deposition angles. (g) Real-time current change of self-powered gas sensors for 2% H_2 gas with different deposition angles.

PUA nanograting film has an asymmetric structure in which the Pd is deposited on the top and on only one side of the PUA nanograting structure. Because of this asymmetric Pd nanostructure, the proposed sensor device can optically detect H_2 gas in a highly reliable manner by exploiting changes of the optical transmittance, without external power (Figure 1b). When ambient visible light is incident on the sensing film, a certain amount of the light is transmitted through gaps between adjacent Pd-PUA nanograting, and it can generate current output in the photovoltaic cell underneath (upper panel in Figure 1b). When H_2 gas meets Pd, the H_2 molecules are decomposed into hydrogen atoms that diffuse into the Pd lattice, resulting in Pd hydrogenation [$Pd + H_2 \rightarrow PdH_x$]. When this occurs, many physical and chemical changes in the Pd occur, including volumetric expansion due to changes in the lattice.[13,18,29−31] In the proposed sensor, because the Pd covers the top and only one side of the PUA nanograting, the PUA nanograting structures become warped on one side by the volumetric expansion of Pd (lower panel in Figure 1b). This chemo-mechanical deformation of the Pd-PUA nanograting blocks some of the incoming light, causing a change in the current output of the photovoltaic cell. Moreover, the deformation of the Pd-PUA nanograting varies according to how much H_2 is absorbed, and thus the concentration of H_2 gas can be detected by measuring the level of output current of the photovoltaic cell, without need for an external power source. To theoretically confirm the feasibility of the proposed concept, we performed FEM simulation (COMSOL Inc., USA), considering a PUA nanograting substrate with a Pd nanostructure on only the top and the side wall of the nanograting. For the asymmetric Pd nanostructure, a 100 nm-thick Pd film was designed as it is formed using the glancing angle deposition method ($\theta = 45°$) on a nanograting substrate (150 nm line, 250 nm space, and 250 nm height), a practical method to fabricate Pd-PUA nanograting films in real experiments (Figure S1). Then, a different volumetric expansion of Pd with respect to the concentration of H_2 was applied for the simulation, considering the previously reported values.[35] Figure 1c shows the results of the FEM simulation. When the volumetric expansion of Pd is generated by H_2, a *x*-axial displacement is induced by the bending of PUA. The *x*-displacement of Pd-PUA was negligible at very low concentrations of H_2, but it was significantly increased as the concentration of H_2 increased. The *x*-displacement of Pd-PUA is 1.6 nm at 0.5% of H_2 (Figure 1c,(i)), but it becomes ~20 nm at 2% of H_2 concentration (Figure 1c,(ii)). Using this FEM simulation method, we further calculated a relative change of Pd

https://dx.doi.org/10.1021/acsnano.0c05476
ACS Nano 2020, 14, 16813−16822

gap, between the adjacent Pd-PUA nanograting, to the original Pd gap ($\Delta w/w_0$) with respect to the H_2 concentration (Figure 1c,(iii)). From the calculation result, we confirmed that the detectable x-displacement change can occur at the Pd-PUA nanograting by the H_2 gas, resulting in the optical transmission change based H_2 gas detection with the self-powered manner, as we proposed. It is worthwhile to note that the simulation was conducted by considering small sizes of Pd-PUA nanograting film ($w \times l \times t$ = 3500 nm × 4000 nm × 400 nm), because real Pd-PUA nanograting films have the same regular structure. Details about this simulation are provided in the "Numerical simulation of Pd expansion" section in the Supporting Information.

To demonstrate the proposed sensor, we developed a large-area nanofabrication process combining nanoimprint lithography and vacuum deposition methods. First, a 400 nm pitch (150 nm line and 250 nm space) PUA nanograting film (2 × 2.5 cm^2) was fabricated using nanoimprint lithography.[34] The line width and space of the PUA nanograting film were the smallest dimensions that can be made through conventional KrF photolithography for the nanoimprinting template fabrication. The small line width of the nanograting can reduce the moment of inertia of the nanograting and maximize the deformation (Δw) by the volume expansion of Pd (Figure S2). Also, the small space of the nanograting can increase the relative change of the Pd gap ($\Delta w/w_0$), even with the same deformation. Next, on the PUA nanograting film with small line width and space, electron beam evaporation of Pd was performed using a glancing angle deposition method to deposit the Pd only on the top surface and one side of each nanograting. Then, the fabricated Pd-PUA nanograting film and photovoltaic cell were assembled using an adhesive tape. The detailed fabrication process is summarized in Figure S1. Scanning electron microscope (SEM) images of the original PUA nanograting film are shown in Figure S3, and the electrical properties of the photovoltaic cell are shown in Figure S4. Furthermore, the experimental details on the PUA nanograting film and photovoltaic cell are shown in the Methods section. An optical image and SEM image of the fabricated device are shown in Figure 1d,e, respectively. Since the proposed fabrication method is fully based on the nanoimprint lithography and vacuum deposition methods, the asymmetric Pd nanostructure on the PUA nanograting was successfully formed with high uniformity, as shown in Figure 1e (glanced deposition angle = 45°, thickness = 100 nm). Top and cross-sectional images of the fabricated Pd-PUA film are shown in the upper and lower panels, respectively, of Figure 1e. Only when taking a cross-sectional SEM image, the passivation layer (*in situ* Pt deposition) was deposited on a local area of Pd-nanograting to prevent a direct damage during focused ion beam (FIB) milling (Figure S5). Besides, since the proposed fabrication process only uses top-down approaches such as nanoimprint process and electron beam evaporation, Pd-PUA nanograting structures can be fabricated reliably with high uniformity and reproducibility, as shown in Figures S6 and S7. Thanks to the uniformly defined nanogaps between each Pd nanostructure, ambient light can penetrate the Pd-PUA nanograting film and generate an output current in the photovoltaic cell (Figure S8).

In the proposed device, the angle of Pd deposition (θ, Figure 1c) is very important, because different shapes of Pd-PUA nanograting film are fabricated by varying the deposition angles (Figure 2a), and these finally determine the H_2 gas sensing performance of the device. For example, by using a smaller deposition angle, a thicker but shallower structure Pd is deposited on the side wall of the PUA nanograting, while a thinner and deeper structure of Pd is formed on the side wall by using a larger deposition angle (Figure 2b). These different shapes of the Pd nanostructures generate different mechanical forces that warp the nanograting. To theoretically predict the chemo-mechanical deformation of the Pd-PUA nanograting with respect to the deposition angle, we performed a numerical analysis based on FEM simulation. In the simulation, we first designed various Pd-PUA nanograting structures, considering different deposition angles from 5° to 85° with 50 nm-thick deposition and calculated the Pd gap (w_0) between the Pd-PUA nanostructures in air condition (Figure S9). Then, we calculated the changed Pd gap (w_{H_2}) of the Pd nanostructures, deposited by different angles (θ), according to the reaction with H_2 gas. For the numerical simulation, we applied a volume expansion of the Pd by 10.9% because of the increase of the Pd lattice constant by 3.5%, which assumes that the deposited Pd is fully transformed into the β-phase PdH_x.[35,36] Figure 2c shows visualized FEM simulation results. As the angle of the Pd deposition became larger, more x-displacement is generated at the Pd-PUA nanograting. The initial Pd gap between Pd-PUA nanograting and the change of Pd gap by the H_2 gas are plotted in Figure 2d,e, respectively. As the deposition angle increases, the initial Pd gap and transmittance increase monotonically (Figure S10). This increase is also observed in the changed Pd gap by H_2, however, there is an inflection point at θ = 45°. Before the 45° deposition angle, the changed Pd gap largely increases as the deposition angle increases, but a sudden decrease of the changed Pd gap is calculated at the deposition angle larger than 45°. Because of this inflection point, the performance of the device can have an optimum point in gas sensing. We further calculated the normalized value of the Pd gap change ($|\Delta w/w_0|$, $\Delta w = w_{H_2} - w_0$), implying the transmission of the light through the Pd-PUA nanograting film in H_2 gas condition. The normalized value of the Pd gap change is calculated and set to increase continuously as the deposition angle increases from 5° to 45°; it reaches a maximum ($|\Delta w/w_0|$ = 0.09) at 45° and then decreases as the angle increases beyond 45° (upper panel in Figure 2f). We understand this result with the maximum x-axial stress when the deposition angle is 45°. At this deposition angle, the same thickness of Pd is deposited on the top and the side-wall of the PUA nanograting, and this structure is the most favorable for achieving maximum x-axial displacement of the nanograting structure. Details about the theoretical calculation, including FEM simulation, are shown in Figure S11. To experimentally confirm the results of the theoretical design optimization, we fabricated four different Pd-PUA nanograting films with various deposition angles (30°, 40°, 45°, and 70°) and measured the normalized output current change ($(I - I_0)/I_0$) by the 2% H_2 gas exposure of each sample (Figure 2g). The experimental details are shown in Figure S12 and in the Methods section. The experimental results highly correspond to the theoretical calculations, as shown in Figure 2f. The measured normalized output current changes are 0.029, 0.060, 0.080, and 0.023 for the deposition angles of 30°, 40°, 45°, and 70°, respectively. Maximum normalized current change ($|(I - I_0)/I_0|$ = 0.080) is also achieved when the deposition angle is 45°, and the tendency of the current change matches well with the numerical simulation results (upper panel in Figure 2f).

The thickness of the deposited Pd (d) can also influence the sensing performance. From the performed FEM simulation considering different thicknesses of Pd, we confirmed the

https://dx.doi.org/10.1021/acsnano.0c05476
ACS Nano 2020, 14, 16813−16822

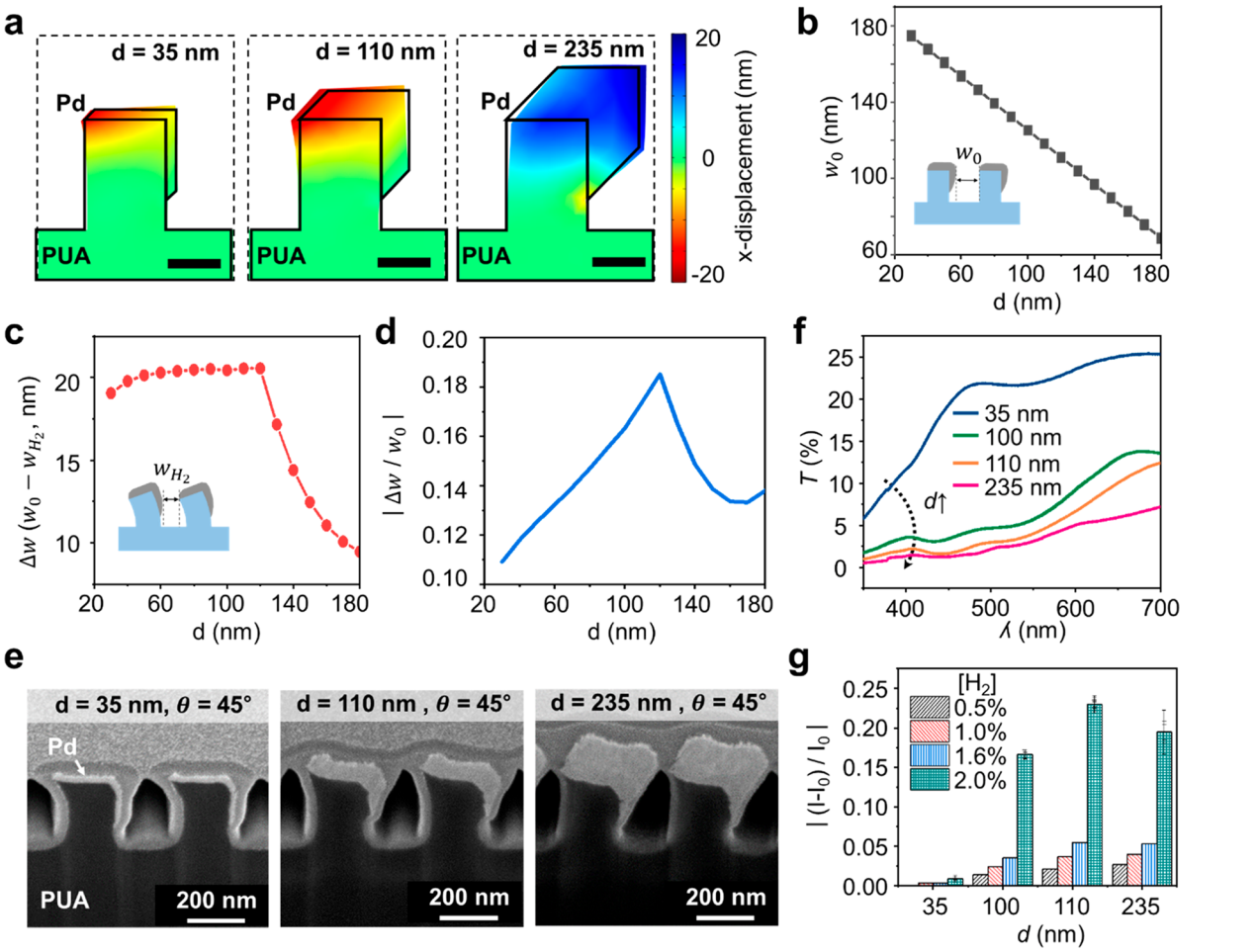

Figure 3. (a) FEM simulation results for the deformation of Pd-PUA nanograting films deposited with various Pd thickness in the 2% H_2 gas. The *x*-axial displacement is presented with a rainbow color map (scale bar = 100 nm). (b) Pd gap of Pd-PUA nanograting according to Pd thickness. (c) Simulation results of the change in the Pd gap of Pd-PUA nanograting deposited with various Pd thicknesses in 2% H_2 gas. (d) The rate of change in the Pd gap of Pd-PUA nanograting films according to Pd thickness. (e) Cross-sectional SEM images of Pd-PUA nanogratings with various Pd thicknesses. (f) Transmittance of various Pd-PUA nanograting films. (g) Current change according to H_2 gas concentrations in self-powered gas sensors with various Pd thicknesses.

significantly different chemo-mechanical displacement of the nanograting (Figure 3a). To specifically understand the influence of the thickness of the Pd on the sensing performance, we also performed the numeric analysis based on the FEM simulation. It is worthy to note that the thickness simulation was performed with the deposition angle of Pd at 45°, and a volume-expansion of 10.9% was applied to the Pd layer to consider the chemo-mechanical displacement. As the deposition thickness increased, the gap between adjacent Pd-PUA nanograting structures (w_0) became narrower (Figure 3b). Even though the initial gap between adjacent Pd-PUA nanograting structures decreases, the *x*-displacement by Pd volumetric expansion ($\Delta w = w_0 - w_{H_2}$) did not show a significant increase as the thickness of Pd increased from 30 to 110 nm; the *x*-displacement was about 20 nm in this thickness range (Figure 3c). However, the large decrease of *x*-displacement was obtained when the thickness of Pd was thicker than 110 nm (Figure 3c). We understand these phenomena with a diffusion limitation of H_2 into Pd (~100 nm).[33] Since no more Pd can be converted into PdH_x in the entire Pd layer in the thicker Pd nanostructure (d > 100 nm), nonconverted Pd generates a higher bending moment of inertia, which inhibits warping of the nanograting structure. The *x*-displacements by the PdH_x conversion in different thickness of Pd nanostructures are shown in Figure S13 in detail. Since the initial gap is monotonically decreased and the *x*-displacement of the nanograting shows the sudden decrease as the deposition-thickness increases above 110 nm, there is also an optimum point in thickness. We calculated the theoretical normalized Pd gap change by the volumetric expansion ($|\Delta w/w_0|$, $\Delta w = w_{H_2} - w_0$) and confirmed the optimum value about $|\Delta w/w_0| = 0.18$, when the thickness of Pd was 110 nm (Figure 3d). We further experimentally confirmed the optimum point in thickness. For the experiment, we demonstrated various types of Pd-PUA nanograting structures, in which the thickness of the Pd thin film varied from 35 to 100, 110, and 235 nm. Cross-sectional SEM images are shown in Figure 3e. From an optical transmission measurement, it is confirmed that a significant light can reach to the photovoltaic cell through the 235 nm-thick Pd-polymer nanograting film (Figure 3f). Figure 3g shows the normalized output current changes (response = $|(I - I_0)/I_0|$) of each sample with respect to various H_2 gas concentrations. In all cases, the responses increased as the concentration of H_2 gas increased, and a significantly large response is observed at 2.0% of H_2 gas. From these results, it can be seen that all devices operated well *via* the proposed chemo-mechanical mechanism, regardless of the thickness. It should be noted that the sudden increase of the

https://dx.doi.org/10.1021/acsnano.0c05476
ACS Nano 2020, 14, 16813−16822

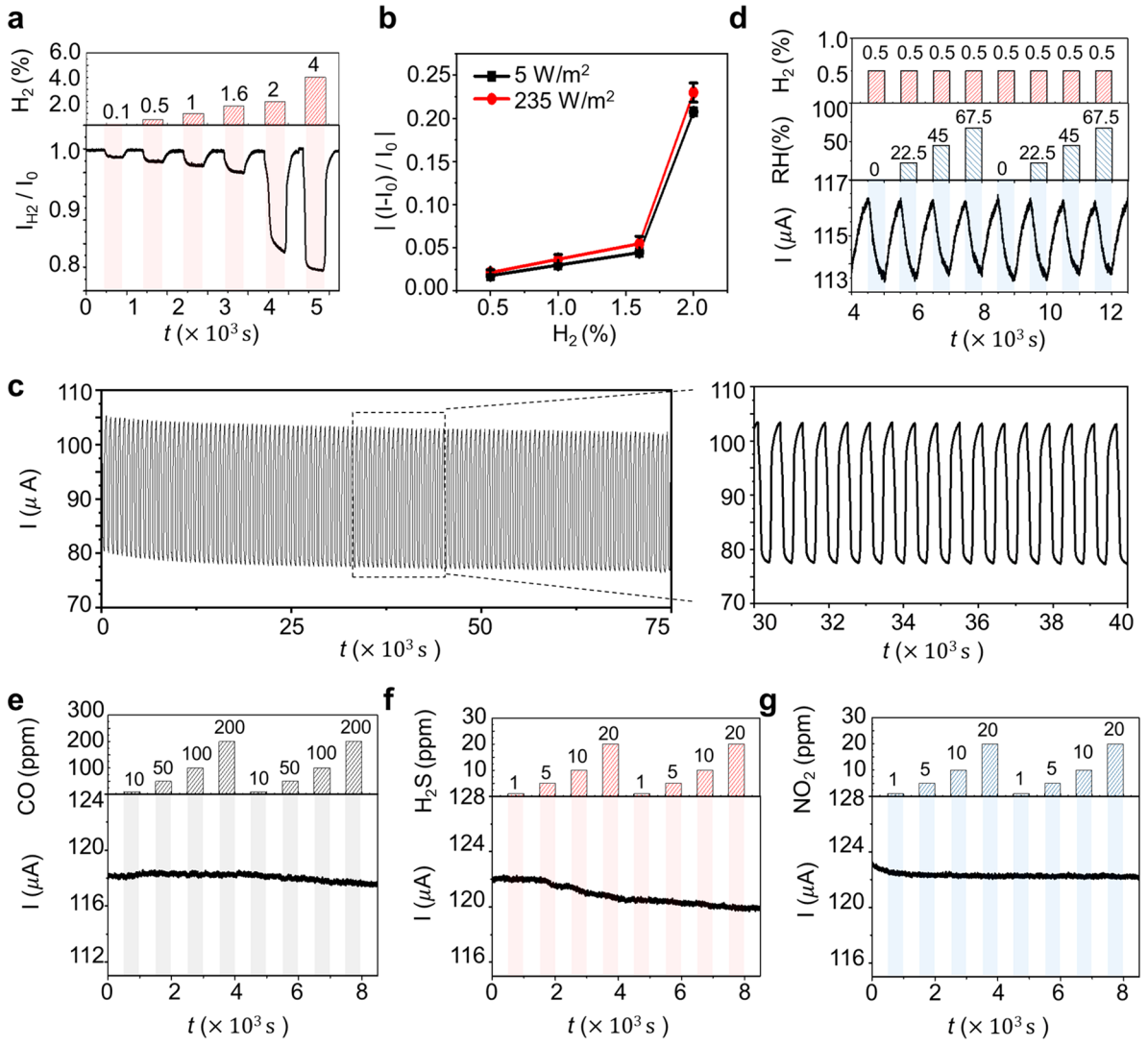

Figure 4. Characterization of a self-powered gas sensor with a Pd thickness of 110 nm and deposition angle of 45°: (a) Real-time gas sensing results for various H_2 gas concentrations, (b) current change according to various H_2 gas concentrations with incident light intensities of 5 W/m^2 and 235 W/m^2, (c) real-time current change for reliability test in response to 2% H_2 gas over 125 cycles, (d) current change according to 0.5% H_2 gas exposure at various humidity conditions, and (e−g) real-time sensor response to various gases such as CO (10, 50, 100, and 200 ppm) (e), H_2S (1, 5, 10, and 20 ppm) (f), and NO_2 (1, 5, 10, and 20 ppm) (g).

response at 2% of H_2 gas is explained by β-phase Pd hydrogenation (PdH_x), which normally occurs at around 2% of H_2 gas, resulting in larger volume expansion and larger bending moment of inertia than those of the α-phase PdH_x.[35] In spite of this similarity, the quantity of the response is largely different with respect to the thickness of Pd. As the thickness of Pd increases, the response improves (the responses of 35, 100, and 110 nm-thick Pd samples are 0.01, 0.17, and 0.23, respectively, at 2% of H_2 gas). These results can be attributed to the larger bending force induced by the thicker Pd layer. However, the response to 2% H_2 gas is larger for the 110 nm-thick Pd film than for 235 nm-thick Pd film (0.23 and 0.19, respectively), as we theoretically confirmed.

From the above parametric studies, we determined that the proposed device could achieve an optimal design for high sensitivity with a deposition angle of 45° and Pd thickness of 110 nm. Using the optimized device, we performed further investigation of the characteristics of the sensing performances, such as detection limit, reliability, and selectivity. Figure 4a shows the normalized output current change of the device with respect to various concentrations of H_2 gas. When the device was exposed to H_2 gas, the output current dynamically decreased. Normalized current changes (response, $|(I - I_0)/I_0|$) are ∼1.5%, ∼2.8%, ∼3.5%, ∼5.0%, ∼21.5%, and 25.3% when the concentrations of H_2 gas are 0.1%, 0.5%, 1.0%, 1.6%, 2%, and 4%, respectively. The sensitivity, which is defined as the slope of response *vs* concentration curve, can be calculated as 0.03/[H_2]%, 0.41/[H_2]%, and 0.02/[H_2]% in a range of ∼1.6% H_2, 1.6−2% H_2, 2−4% H_2, respectively. Besides, when compared with the small current increase (∼1%) of the flat Pd film in Figure S14, the large current decrease (∼21.5%) of the Pd-PUA nanograting film shows that the decrease of the gap between Pd nanopatterns contributes more to the high sensitivity than the change in the transmittance of Pd film. The sudden increase of the response at 2% of H_2 gas is also explained by the β-phase of PdH_x. Noticeably, the device successfully detects 0.1% H_2 gas, which satisfies the limit of detection for the safety of H_2 gas as required by the United States Department of Energy (DOE).[37] Additionally, with advanced fabrication technologies, if the aspect ratio of the nanograting increases by reducing the width

https://dx.doi.org/10.1021/acsnano.0c05476
ACS Nano 2020, 14, 16813−16822

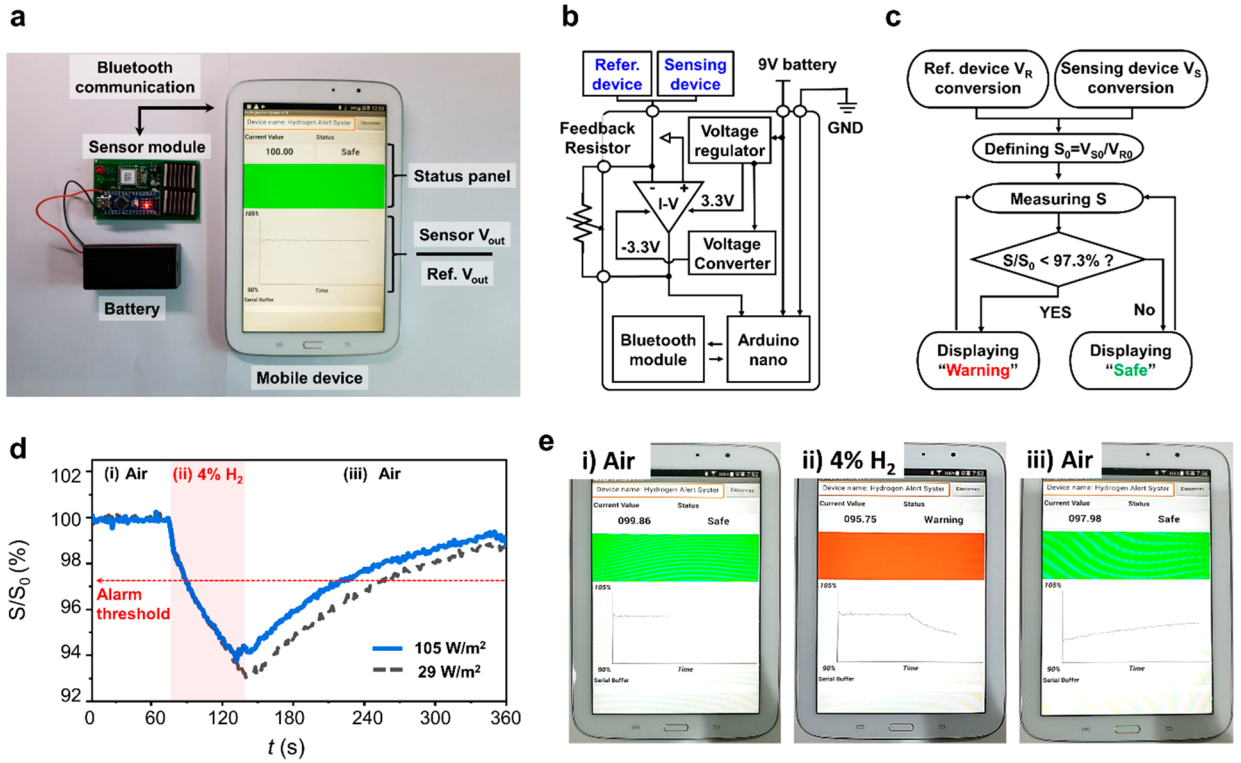

Figure 5. (a) Optical image of Pd-PUA nanograting based self-powered H_2 gas sensing system. (b) Schematic circuit image of Arduino module with Bluetooth, voltage converter, voltage regulator, op-amp, 9 V battery, and two photovoltaic cells. (c) Logic diagram for real-time H_2 gas detection and alarm. (d) Real-time sensing results and (e) alarm results displayed on a mobile device according to changes of environment (*i.e.*, air and 4% H_2 gas, light intensities of 105 W/m^2 and 29 W/m^2).

and increasing the height, we expect that the sensitivity can be improved because the moment of inertia is reduced.

The optical stability of the device was also tested. Using various levels of ambient light power, we evaluated the sensing performance of the device. In spite of different ambient light intensities (5 W/m^2 and 235 W/m^2), the device showed consistent output current changes for various concentrations of H_2 gas (Figure 4b). In addition, the base current in a low light intensity of 5 W/m^2 is 3 μA, which can be sufficiently detected by the ammeter chip of conventional small devices, so it is suitable for use even where there is insufficient light (Figure S15). Furthermore, we can verify through finite-difference time-domain (FDTD) simulation that even if the incident angle of ambient light is different, the transmittance is stably maintained (Figure S16). The reliability of the device was also tested. Under conditions of repetitively changing the concentrations of H_2 gas (2 cycles of 0.5%, 1.0%, 1.5%, and 2.0% of H_2 gas), the device showed a reproducibility of the sensing performance (Figure S17). Besides, the structure of Pd-PUA nanograting remained the same before and after repeated H_2 gas sensing experiments, even though Pd had experienced a volume expansion (Figure S18). Significantly, the device also showed a long-term stability against a high concentration of H_2 gas (2%). During 125 cyclic exposures to 2% H_2 gas, we can see that the width of the crack, caused by the defect during the Pd deposition process, was widened after the cycle test in the top SEM image (Figure S19a). However, the occupied area of the generated cracks was minimal, about 0.7% of the total area. Besides, when the transmittance of crack film was confirmed through FDTD simulation, the transmittance was well maintained with a small deviation of 5% due to a small area of the crack (Figure S19b). As a result, in the experimental results, the base current and the output current changes are also stably maintained with small deviations of 2.0% and 2.9%, respectively (Figure 4c). It should be noted that the long-term reliability of devices under a high concentration of H_2 gas (≥2%) is difficult to be achieved in the conventional Pd-based chemo-resistive-type H_2 gas sensors, because electrical breakdowns can easily be generated by structural degradation and fatigue fracture of Pd (Table S1).[32,38]

The selectivity is a crucial factor for gas sensors, considering that there are abundant gaseous species such as H_2O, CO, H_2S, and NO_2. In order to characterize the sensitivity of the sensor to humidity, gas sensing experiments were conducted with the H_2 gas concentration fixed at 0.5% and the relative humidity (RH) changed to 0, 22.5, 45, and 67.5%, as shown in Figure 4d. The real-time response plot shows almost identical responses (average = 0.020, minimum = 0.019, and maximum = 0.024), regardless of the humidity of the input gas. Even at a high humidity of 80% RH, the sensor response was similar to that in a dry condition, as shown in Figure S20. We understand that the immunity of the sensor against wetting may have been achieved by nanostructures on the film. Our periodic nanostructures can trap an air pocket between structures, as shown in Figure S21a, forming a Cassie−Baxter state in which water cannot enter the structures. The Cassie−Baxter state of the Pd- PUA nanograting structure causes the hydrophobic properties of the high contact angle and small hysteresis in contact angles (the difference between advancing and receding contact angles) even on an inclined surface, as shown in Figure S21b,c. As a result, the hydrophobic property of nanograting can maintain the H_2 absorption of Pd by suppressing the formation of a water layer in a high-humidity environment. Therefore, we can conclude that the proposed H_2 gas sensor is not greatly affected by the humidity changes due to the hydrophobic properties and is

https://dx.doi.org/10.1021/acsnano.0c05476
ACS Nano 2020, 14, 16813−16822

expected to operate stably both in humid and dry conditions. In the cases of metal oxide or Pd-based chemo-resistive H_2 gas sensors, responses are decreased by the adsorption of water molecules under high-humidity conditions.[7,39] In this respect, our proposed sensor shows a very stable H_2 gas sensing response in a variety of humidity conditions. In addition, in terms of stability over varying temperature, the FEM simulation results show that the proportion change of the Pd gap ($\Delta w/w_0$) under 2% H_2 gas is well maintained in the temperature range from 0 to 60 °C (Figure S22a,b). The fabricated PUA substrate stored at 5 and 80 °C for 24 h also maintained initial mechanical properties and cross-sectional SEM image (Figure S22b,c). Therefore, we expect that the proposed sensor can be reliably used in various temperature conditions. We also tested the selectivity of the proposed sensor against various concentrations of CO (10, 50, 100, and 200 ppm), H_2S (1, 5, 10, and 20 ppm), and NO_2 (1, 5, 10, and 20 ppm) gases (Figure 4e–g). For all three gases, no matter what concentration was injected, no change of current output of the photovoltaic cell was noticeable. So far, we have confirmed that the proposed device can detect H_2 gas in a highly reproducible and selective manner. Moreover, thanks to the use of a photovoltaic cell, the proposed device does not require any external energy source. Thus, we think that the proposed concept can be utilized for energy efficient continuous H_2 gas monitoring systems.

Finally, to show the feasibility of the self-powered H_2 gas sensing system, we demonstrated a wireless H_2 gas sensing system (Figure 5a) by modularizing the proposed sensor with other electrical components on a printed circuit board to implement a practical gas sensing system. The module consisted of an Arduino platform, Bluetooth chip, voltage converter, voltage regulator, op-amp, 9 V battery, reference photovoltaic cell, and photovoltaic cell covered by the Pd-PUA nanograting film (Figure 5b). In particular, we used the reference cell, which does not have the Pd-PUA nanograting film, to compensate for the errors due to the varying intensity of ambient light. The stable H_2 gas sensing is performed by calculating a relative value of the output signal of the sensing cell compared to that of the reference cell. Calculation of the outputs of the reference and sensing photovoltaic cells is done by the Arduino system, and the calculated results are transferred to the mobile device by Bluetooth communication. We also programmed the mobile device so that it can show a warning alarm when the signal exceeds a certain threshold value due to the exposure to excessive H_2 gas. The circuit information is explained in the Methods section. To quickly demonstrate this prototype system, we used a 9 V battery for the circuit operation. In the future, by applying a low power circuit, this electrical power can be replaced by that generated from the reference photovoltaic cell. Figure 5c provides a detailed algorithm diagram of the system. First, the output currents from the reference cell (I_R) and sensing photovoltaic cell (I_S) are converted into voltages V_R and V_S, respectively, by a current-to-voltage converter circuit. The ratio of these two voltages in an air environment ($S_0 = V_{S_0}/V_{R_0}$) and that in the presence of H_2 gas ($S = V_S/V_R$) are used to define the threshold to activate the alarm. Specifically, for the monitoring of 4% H_2 gas using an 105 W/m^2 white-light, the alarm is activated when S/S_0 is less than 97.3%, and the alarm is deactivated when S/S_0 is greater than that value. Changes in the signal recorded in the mobile device are shown in Figure 5d. The ratio of S/S_0 decreases when the module is exposed to H_2 gas because the optical transmittance of the sensing film (*i.e.*, Pd-PUA nanograting film) is reduced. Before the signal reaches the threshold, the display of the mobile device shows the message "Safe" with a green light, and when the threshold value is reached, a "Warning" message with a red light appears. Finally, the display shows "Safe" again, when S/S_0 is higher than 97.3% (Figure 5e). To confirm the stability against variation of the ambient light, the H_2 gas sensing performance of the developed module was further tested under a different light condition (intensity = 29 W/m^2). The repetitive and reliable gas sensing is achieved regardless of the light intensity (dashed line in Figure 5d). The video clip about the operating sensor module can be seen in Supporting Information Video S1.

CONCLUSION

In this study, we developed a self-powered H_2 gas sensor using a photovoltaic cell and chemo-mechanically deforming Pd-PUA nanograting structure. The sensor mechanism is based on the change in the optical transmittance of the nanograting structure caused by the expansion of Pd after reaction with H_2 gas, which is then detected by the change of the current output of the photovoltaic cell. This sensor operates by the power of ambient light, thereby requiring no external electrical power. The sensor was able to detect H_2 gas at concentrations as low as 0.1%, with a selectivity against CO, H_2S, and NO_2, and high stability against humidity change. In addition, it showed a high reliability and repeatability, ensuring its applicability to real-life, long-term usage. Furthermore, the proposed sensor showed good sensing performance regardless of the light intensity. Therefore, this sensor can be utilized anywhere, as long as a small amount of visible light exists. Finally, we demonstrated that the developed sensor can be used in portable H_2 gas leakage alarm systems by integrating it with an Arduino platform and wireless communication. Therefore, we expect that this sensor can be used as a self-powered sensor device for detecting H_2 gas leakage in hydrogen stations and industrial sites that frequently use H_2 gas. Also, if another material that can react with a particular target gas and generate mechanical deformation is utilized, the proposed sensing approach can be used to detect other gases, without external electrical power.

METHODS

Fabrication of Pd-PUA Nanograting Film. The fabrication process began with a cm-scale silicon (Si) nanograting template (2 × 2.5 cm^2) made by conventional KrF photolithography. To fabricate the nanograting PUA polymer substrate, a typical nanoimprint lithography process was performed to generate a periodic nanograting pattern with a width of 150 nm and a height of 250 nm. First, UV-curable PUA (HC11M-J5, Minuta Technology Co., Ltd., South Korea) resin and a 50 μm-thick polyethylene terephthalate (PET) backing layer were subsequently formed on the Si nanograting template, and the PUA was cured by 400 mJ I-line (365 nm wavelength) UV exposure. After UV curing, the polymer substrate was peeled off gently from the template (Figure S23). On the fabricated PUA nanograting film, electron beam evaporation of Pd was performed using a glancing angle deposition method to deposit the Pd on only one side of each nanograting structure.

Fabrication of Photovoltaic Cell. The substrate electrode material was a glass (JM International Co., South Korea) coated with indium tin oxide (ITO, 75 nm thickness). For the electron transport layer, a solution was made by mixing zinc acetate dehydrate (1 g, Sigma-Aldrich, USA) and ethanolamine (0.28 g, Sigma-Aldrich, USA) in 2-methoxyethanol (10 mL, Sigma-Aldrich, USA). The mixture was stirred for over 8 h at room temperature and then deposited on the ITO-coated glass substrate by spin coating at 3000 rpm for 30 s. The sample was then heat-treated at 200 °C for 30 min in a box furnace.[40] For the

https://dx.doi.org/10.1021/acsnano.0c05476
ACS Nano 2020, 14, 16813–16822

photoactive layer, *O*-dichlorobenzene (Sigma-Aldrich, USA) and 1,8-diiodooctane (Sigma-Aldrich, USA) were mixed at a ratio of 97:3 as the solvent, and poly-3-hexylthiophene-2,5-diyl (Rieke Metals, USA) and phenyl-C_{61}-butyric acid methyl ester (Nano-C Company, USA) were mixed at a ratio of 1:1 as the solute. The solute was dissolved in the solvent at a concentration of 10 mg/mL. The mixture was spin-coated on the previously fabricated substrate at 2000 rpm for 60 s, and the sample was heat-treated at 150 °C for 10 min.[41] Finally, a hole-transporting layer of molybdenum oxide (10 nm thickness) and silver (150 nm thickness) electrodes were formed by thermal evaporation.

Measurement of Sensor Response to Target Gas under Visible Light. Since the fabricated photovoltaic sensor has a high-energy efficiency in the visible light region, a xenon light source (LAX-C100, Asahi Spectra, Japan) with a visible light filter was set to operate the Pd-PUA nanograting H_2 gas sensor.[42−44] The sensing film with the organic photovoltaic cell was placed in a gas chamber (width: 85 mm, length: 155 mm, height: 40 mm) with a transparent cover, H_2 gas was mixed with a synthetic air (*i.e.*, mixture of N_2 and O_2), and the concentration of the target gas was controlled using a mass flow controller (AFC500, Atovac, South Korea). When measuring gas, the gas flow was kept constant at 500 sccm. The light intensity for the sensor operation was 235 W/m^2 for most of the sensor experiments and 5 W/m^2 for the validity test of sensor operation at a low light intensity. The output current from the photovoltaic cell was measured by a source meter (2400, Keithley, USA) without any voltage input.

Electrical Circuits for the Self-Powered Gas Sensor. The electronic module for the H_2 gas alarm application consisted of two commercial photovoltaic cells (AM-5610CAR, Panasonic-BSG, Japan), an Arduino platform (Pro mini, Arduino.CC, USA), a Bluetooth module (FB155BC, Firmtech, South Korea), a voltage converter (TL7660, Texas Instruments, USA), a voltage regulator (MIC5219, Microchip, USA), an operational amplifier (op-amp, LM7332, Texas Instruments, USA), and a 9 V battery. One photovoltaic cell was covered by the Pd-PUA nanograting film for gas sensing, and another was not covered to measure the incident light intensity as a reference. The output currents from the photovoltaic cells were converted to voltage values using a current-to-voltage converter circuit including op-amp, because the Arduino can read voltage values only. If the change ratio between the output voltages of the two cells was larger than a predetermined threshold value, an alarm was made by a message and a color change in the mobile device.

ASSOCIATED CONTENT

Supporting Information

The Supporting Information is available free of charge at https://pubs.acs.org/doi/10.1021/acsnano.0c05476.

Figures show additional information such as the fabrication process and experimental results (PDF)

Movie S1: The demonstration of a wireless H_2 gas sensing system (MP4)

AUTHOR INFORMATION

Corresponding Authors

Inkyu Park − *Department of Mechanical Engineering, Korea Advanced Institute of Science and Technology (KAIST), Daejeon 34141, Republic of Korea;* orcid.org/0000-0001-5761-7739; Email: inkyu@kaist.ac.kr

Jun-Bo Yoon − *School of Electrical Engineering, Korea Advanced Institute of Science and Technology (KAIST), Daejeon 34141, Republic of Korea;* orcid.org/0000-0002-9447-3807; Email: jbyoon@kaist.ac.kr

Junsuk Rho − *Department of Mechanical Engineering and Department of Chemical Engineering, Pohang University of Science and Technology (POSTECH), Pohang 37673, Republic of Korea;* orcid.org/0000-0002-2179-2890; Email: jsrho@postech.ac.kr

Authors

Min-Ho Seo − *School of Biomedical Convergence Engineering, College of Information and Biomedical Engineering, Pusan National University, Yangsan-si 43241, Gyeongsangnam-do, Republic of Korea*

Kyungnam Kang − *Department of Mechanical Engineering, Korea Advanced Institute of Science and Technology (KAIST), Daejeon 34141, Republic of Korea*

Jae-Young Yoo − *School of Electrical Engineering, Korea Advanced Institute of Science and Technology (KAIST), Daejeon 34141, Republic of Korea*

Jaeho Park − *Department of Mechanical Engineering, Korea Advanced Institute of Science and Technology (KAIST), Daejeon 34141, Republic of Korea;* orcid.org/0000-0002-0213-8076

Jae-Shin Lee − *Samsung Electronics Co., Ltd., Suwon 18448, Republic of Korea*

Incheol Cho − *Department of Mechanical Engineering, Korea Advanced Institute of Science and Technology (KAIST), Daejeon 34141, Republic of Korea*

Beom-Jun Kim − *School of Electrical Engineering, Korea Advanced Institute of Science and Technology (KAIST), Daejeon 34141, Republic of Korea*

Yongrok Jeong − *Department of Mechanical Engineering, Korea Advanced Institute of Science and Technology (KAIST), Daejeon 34141, Republic of Korea*

Jung-Yong Lee − *School of Electrical Engineering, Korea Advanced Institute of Science and Technology (KAIST), Daejeon 34141, Republic of Korea;* orcid.org/0000-0002-5347-8230

Byeongsu Kim − *School of Electrical Engineering, Korea Advanced Institute of Science and Technology (KAIST), Daejeon 34141, Republic of Korea*

Complete contact information is available at: https://pubs.acs.org/10.1021/acsnano.0c05476

Author Contributions

[∇]These authors contributed equally.

Notes

The authors declare no competing financial interest.

ACKNOWLEDGMENTS

This work was supported by the National Research Foundation of Korea (NRF) grant funded by the Korean government (MSIT) (no. 2015R1A5A1037668). This research was also supported by Nano·Material Technology Development Program through NRF funded by the Ministry of Science, ICT, and Future Planning (no. 2009-0082580). J.R. acknowledges the POSTECH-Samsung Electronics research center funded by Samsung Electronics Co., Ltd. The EDA tool was supported by the IC Design Education Center (IDEC), Republic of Korea.

REFERENCES

(1) Crabtree, G. W.; Dresselhaus, M. S.; Buchanan, M. V. The Hydrogen Economy. *Phys. Today* **2004**, *57* (12), 39−44.

(2) Marbán, G.; Valdés-Solís, T. Towards the Hydrogen Economy? *Int. J. Hydrogen Energy* **2007**, *32* (12), 1625−1637.

(3) Ahn, J.-H.; Yun, J.; Moon, D.-I.; Choi, Y.-K.; Park, I. Self-Heated Silicon Nanowires for High Performance Hydrogen Gas Detection. *Nanotechnology* **2015**, *26* (9), 095501.

(4) Lim, M. A.; Kim, D. H.; Park, C.-O.; Lee, Y. W.; Han, S. W.; Li, Z.; Williams, R. S.; Park, I. A New Route toward Ultrasensitive, Flexible

Chemical Sensors: Metal Nanotubes by Wet-Chemical Synthesis along Sacrificial Nanowire Templates. *ACS Nano* **2012**, *6* (1), 598−608.
(5) Ramachandran, R.; Menon, R. K. An Overview of Industrial Uses of Hydrogen. *Int. J. Hydrogen Energy* **1998**, *23* (7), 593−598.
(6) Hunaidi, O.; Chu, W.; Wang, A.; Guan, W. Detecting Leaks in Plastic Pipes. *J. - Am. Water Works Assoc.* **2000**, *92* (2), 82−94.
(7) Choi, S.-J.; Chattopadhyay, S.; Kim, J. J.; Kim, S.-J.; Tuller, H. L.; Rutledge, G. C.; Kim, I.-D. Coaxial Electrospinning of WO_3 Nanotubes Functionalized with Bio-Inspired Pd Catalysts and Their Superior Hydrogen Sensing Performance. *Nanoscale* **2016**, *8* (17), 9159−9166.
(8) Hübert, T.; Boon-Brett, L.; Black, G.; Banach, U. Hydrogen Sensors-A Review. *Sens. Actuators, B* **2011**, *157* (2), 329−352.
(9) Samerjai, T.; Tamaekong, N.; Liewhiran, C.; Wisitsoraat, A.; Tuantranont, A.; Phanichphant, S. Selectivity towards H_2 Gas by Flame-Made Pt-Loaded WO_3 Sensing Films. *Sens. Actuators, B* **2011**, *157* (1), 290−297.
(10) Wongchoosuk, C.; Wisitsoraat, A.; Phokharatkul, D.; Tuantranont, A.; Kerdcharoen, T. Multi-Walled Carbon Nanotube-Doped Tungsten Oxide Thin Films for Hydrogen Gas Sensing. *Sensors* **2010**, *10* (8), 7705−7715.
(11) Lee, E.-B.; Hwang, I.-S.; Cha, J.-H.; Lee, H.-J.; Lee, W.-B.; Pak, J. J.; Lee, J.-H.; Ju, B.-K. Micromachined Catalytic Combustible Hydrogen Gas Sensor. *Sens. Actuators, B* **2011**, *153* (2), 392−397.
(12) Javahiraly, N. Review on Hydrogen Leak Detection: Comparison between Fiber Optic Sensors Based on Different Designs with Palladium. *Opt. Eng.* **2015**, *54* (3), 030901.
(13) Mubeen, S.; Zhang, T.; Yoo, B.; Deshusses, M. A.; Myung, N. V. Palladium Nanoparticles Decorated Single-Walled Carbon Nanotube Hydrogen Sensor. *J. Phys. Chem. C* **2007**, *111* (17), 6321−6327.
(14) Kong, J.; Chapline, M. G.; Dai, H. Functionalized Carbon Nanotubes for Molecular Hydrogen Sensors. *Adv. Mater.* **2001**, *13* (18), 1384−1386.
(15) Chen, Z.; Jie, J.; Luo, L.; Wang, H.; Lee, C.; Lee, S. Applications of Silicon Nanowires Functionalized with Palladium Nanoparticles in Hydrogen Sensors. *Nanotechnology* **2007**, *18* (34), 345502.
(16) Nah, J.; Kumar, S. B.; Fang, H.; Chen, Y.-Z.; Plis, E.; Chueh, Y.-L.; Krishna, S.; Guo, J.; Javey, A. Quantum Size Effects on the Chemical Sensing Performance of Two-Dimensional Semiconductors. *J. Phys. Chem. C* **2012**, *116* (17), 9750−9754.
(17) Yun, J.; Jin, C. Y.; Ahn, J.-H.; Jeon, S.; Park, I. A Self-Heated Silicon Nanowire Array: Selective Surface Modification with Catalytic Nanoparticles by Nanoscale Joule Heating and Its Gas Sensing Applications. *Nanoscale* **2013**, *5* (15), 6851−6856.
(18) Ahn, J.-H.; Yun, J.; Choi, Y.-K.; Park, I. Palladium Nanoparticle Decorated Silicon Nanowire Field-Effect Transistor with Side-Gates for Hydrogen Gas Detection. *Appl. Phys. Lett.* **2014**, *104* (1), 013508.
(19) Kolmakov, A.; Klenov, D.; Lilach, Y.; Stemmer, S.; Moskovits, M. Enhanced Gas Sensing by Individual SnO_2 Nanowires and Nanobelts Functionalized with Pd Catalyst Particles. *Nano Lett.* **2005**, *5* (4), 667−673.
(20) Choi, K.-W.; Lee, J.-S.; Seo, M.-H.; Jo, M.-S.; Yoo, J.-Y.; Sim, G. S.; Yoon, J.-B. Batch-Fabricated CO Gas Sensor in Large-Area (8-in.) with Sub-10 mW Power Operation. *Sens. Actuators, B* **2019**, *289*, 153−159.
(21) Burgues, J.; Marco, S. Low Power Operation of Temperature-Modulated Metal Oxide Semiconductor Gas Sensors. *Sensors* **2018**, *18* (2), 339.
(22) Yang, D.; Fuadi, M. K.; Kang, K.; Kim, D.; Li, Z.; Park, I. Multiplexed Gas Sensor Based on Heterogeneous Metal Oxide Nanomaterial Array Enabled by Localized Liquid-Phase Reaction. *ACS Appl. Mater. Interfaces* **2015**, *7* (19), 10152−10161.
(23) Bai, H.; Shi, G. Gas Sensors Based on Conducting Polymers. *Sensors* **2007**, *7* (3), 267−307.
(24) Nguyen, L. Q.; Phan, P. Q.; Duong, H. N.; Nguyen, C. D.; Nguyen, L. H. Enhancement of NH_3 Gas Sensitivity at Room Temperature by Carbon Nanotube-Based Sensor Coated with Co Nanoparticles. *Sensors* **2013**, *13* (2), 1754−1762.
(25) Lee, J.-S.; Seo, M.-H.; Choi, K.-W.; Yoo, J.-Y.; Jo, M.-S.; Yoon, J.-B. Stress-Engineered Palladium Nanowires for Wide Range (0.1%-3.9%) of H_2 Detection with High Durability. *Nanoscale* **2019**, *11* (35), 16317−16326.
(26) Yang, D.; Kim, D.; Ko, S. H.; Pisano, A. P.; Li, Z.; Park, I. Focused Energy Field Method for the Localized Synthesis and Direct Integration of 1D Nanomaterials on Microelectronic Devices. *Adv. Mater.* **2015**, *27* (7), 1207−1215.
(27) Cho, I.; Kang, K.; Yang, D.; Yun, J.; Park, I. Localized Liquid-Phase Synthesis of Porous SnO_2 Nanotubes on MEMS Platform for Low-Power, High Performance Gas Sensors. *ACS Appl. Mater. Interfaces* **2017**, *9* (32), 27111−27119.
(28) DiMeo, F., Jr.; Chen, S.; Chen, P.; Neuner, J.; Roerhl, A.; Welch, J. MEMS-Based Hydrogen Gas Sensors. *Sens. Actuators, B* **2006**, *117* (1), 10−16.
(29) Lewis, F. *The Palladium Hydrogen. System*; Academic Press: London, 1967; p 178.
(30) Favier, F.; Walter, E. C.; Zach, M. P.; Benter, T.; Penner, R. M. Hydrogen Sensors and Switches from Electrodeposited Palladium Mesowire Arrays. *Science* **2001**, *293* (5538), 2227−2231.
(31) Li, X.; Liu, Y.; Hemminger, J. C.; Penner, R. M. Catalytically Activated Palladium@ Platinum Nanowires for Accelerated Hydrogen Gas Detection. *ACS Nano* **2015**, *9* (3), 3215−3225.
(32) Yang, F.; Taggart, D. K.; Penner, R. M. Fast, Sensitive Hydrogen Gas Detection Using Single Palladium Nanowires that Resist Fracture. *Nano Lett.* **2009**, *9* (5), 2177−2182.
(33) Lee, E.; Lee, J. M.; Koo, J. H.; Lee, W.; Lee, T. Hysteresis Behavior of Electrical Resistance in Pd Thin Films during the Process of Absorption and Desorption of Hydrogen Gas. *Int. J. Hydrogen Energy* **2010**, *35* (13), 6984−6991.
(34) Yoo, J.-Y.; Seo, M.-H.; Lee, J.-S.; Choi, K.-W.; Jo, M.-S.; Yoon, J.-B. Industrial Grade, Bending-Insensitive, Transparent Nanoforce Touch Sensor *via* Enhanced Percolation Effect in a Hierarchical Nanocomposite Film. *Adv. Funct. Mater.* **2018**, *28* (42), 1804721.
(35) Suleiman, M.; Jisrawi, N.; Dankert, O.; Reetz, M.; Bähtz, C.; Kirchheim, R.; Pundt, A. Phase Transition and Lattice Expansion during Hydrogen Loading of Nanometer Sized Palladium Clusters. *J. Alloys Compd.* **2003**, *356*, 644−648.
(36) Offermans, P.; Tong, H.; Van Rijn, C.; Merken, P.; Brongersma, S.; Crego-Calama, M. Ultralow-Power Hydrogen Sensing with Single Palladium Nanowires. *Appl. Phys. Lett.* **2009**, *94* (22), 223110.
(37) Buttner, W. J.; Post, M. B.; Burgess, R.; Rivkin, C. An Overview of Hydrogen Safety Sensors and Requirements. *Int. J. Hydrogen Energy* **2011**, *36* (3), 2462−2470.
(38) Pierce, D.; Brusius, P. Electromigration: A Review. *Microelectron. Reliab.* **1997**, *37* (7), 1053−1072.
(39) Cho, M.; Zhu, J.; Kim, H.; Kang, K.; Park, I. Half-Pipe Palladium Nanotube-Based Hydrogen Sensor Using a Suspended Nanofiber Scaffold. *ACS Appl. Mater. Interfaces* **2019**, *11* (14), 13343−13349.
(40) Cha, H.-C.; Huang, Y.-C.; Hsu, F.-H.; Chuang, C.-M.; Lu, D.-H.; Chou, C.-W.; Chen, C.-Y.; Tsao, C.-S. Performance Improvement of Large-Area Roll-to-Roll Slot-Die-Coated Inverted Polymer Solar Cell by Tailoring Electron Transport Layer. *Sol. Energy Mater. Sol. Cells* **2014**, *130*, 191−198.
(41) He, Y.; Shao, M.; Xiao, K.; Smith, S. C.; Hong, K. High-Performance Polymer Photovoltaics Based on Rationally Designed Fullerene Acceptors. *Sol. Energy Mater. Sol. Cells* **2013**, *118*, 171−178.
(42) Dennler, G.; Scharber, M. C.; Brabec, C. J. Polymer-Fullerene Bulk-Heterojunction Solar Cells. *Adv. Mater.* **2009**, *21*, 1323−1338.
(43) Yang, X.; Loos, J.; Veenstra, S. C.; Verhees, W. J. H.; Wienk, M.; Kroon, J. M.; Michels, M. A. J.; Janssen, R. A. J. Nanoscale Morphology of High-Performance Polymer Solar Cells. *Nano Lett.* **2005**, *5* (4), 579−583.
(44) LAX-C100 Xenon Light Source datasheet, https://www.asahi-spectra.com/opticalinstrument/download/laxc100_techinfo.pdf (accessed October 1, 2020).

https://dx.doi.org/10.1021/acsnano.0c05476
ACS Nano 2020, 14, 16813−16822